Composite Structures 171 (2017) 335–344

Contents lists available at ScienceDirect

Composite Structures

journal homepage: www.elsevier.com/locate/compstruct

Free vibration analysis of sandwich beams with honeycomb-corrugation hybrid cores

Zhi-jia Zhang [a,b], Bin Han [b,c], Qian-cheng Zhang [a,b,*], Feng Jin [a,b,*]

[a] State Key Laboratory for Strength and Vibration of Mechanical Structures, Xi'an Jiaotong University, Xi'an 710049, PR China
[b] MOE Key Laboratory for Multifunctional Materials and Structures, Xi'an Jiaotong University, Xi'an 710049, PR China
[c] School of Mechanical Engineering, Xi'an Jiaotong University, Xi'an 710049, PR China

ARTICLE INFO

Article history:
Received 10 February 2017
Accepted 10 March 2017
Available online 14 March 2017

Keywords:
Honeycomb-corrugation hybrid core
Sandwich beam
Free vibration
Equivalent model

ABSTRACT

The vibration performance of sandwich beams with honeycomb-corrugation hybrid cores was investigated in this paper. The method of homogenization was employed to obtain the equivalent macroscopic stiffness of honeycomb-corrugation hybrid cores. Finite element methods and modal analysis techniques have been used to predict their vibration characteristics (*i.e.* their natural frequencies and mode shapes). It is shown that in most cases the predictions by using the equivalent homogenization model (2D model) agree well with the experimental and three-dimensional finite element calculated results. For sandwich beams with corrugated cores, the filling honeycomb not only enhances their flexural rigidity and increases their natural frequency of higher orders, but also more or less eliminates the anisotropy of the structural stiffness and suppresses the local modes of vibration. In addition, considering mass efficiency, a dimensionless frequency parameter was proposed. It was found that the frequency parameter has different sensitivity to the geometry parameters, *i.e.* the slenderness ratio of corrugated member, the face sheet thickness ratio and the relative density of filling honeycomb.

1. Introduction

Due to their multi-functional characteristic, periodic cellular metal sandwich structural body comprising such as honeycomb or corrugated core have been being widely used in such engineering application fields as aerospace, high speed transportation, and submarine [1,2], which put forward the higher demand on physically limited space. However there is still a large amount of space in corrugated, honeycombed and pyramidal cores [3–5] at millimeter scale.

In order to improve their weight and space efficiency, many hybrid cores structures had been constructed to enhance mechanical properties of sandwich structures [6]. Originally filled polymer foams were applied to construct hybrid sandwich cores such as pin-reinforced foams [7–9], polymer foam-filled reinforced composite lattices [10,11], polymer foam-filled metallic corrugation [12–15] and polymer foam-filled honeycomb [16]. However the outcome was disappointing, as sandwiches with polymeric foam-filled cores only performed nearly as well as sandwiches of the same weight with unfilled cores. In recent years, metallic foams having higher strength than polymer foam have already been used as a filling material to form aluminum foam-filled metallic tubes [17] and metal foam-filled metallic corrugation [18–20]. It was surprising that metal foam filling could greatly increase the strength and energy absorption of sandwich structures. The completely different results were attributed to an underlying mechanism: the lateral support to the core member not by weakly but strongly filled foam, altering the deformation modes and considerably delaying core member buckling. However, the weight and space efficiency of new composite structures can still not be carried out adequately. The main reason is that filled foams in these structures have been enhanced next to nothing by such ordered porous materials as metallic corrugation. In order to improve structure efficiency in composite porous structures, new idea about honeycomb-filled corrugated core has been proposed [1,21], which significantly increases the weight and space efficiency of sandwich structures by mutual enhancement of corrugated member and filled honeycomb, *i.e.* the mutual constraint of corrugated member and honeycomb cell walls against buckling changes the deformation mode of structure.

* Corresponding authors at: State Key Laboratory for Strength and Vibration of Mechanical Structures, Xi'an Jiaotong University, Xi'an 710049, PR China (Q.-c. Zhang and F. Jin).

E-mail addresses: zqc111999@mail.xjtu.edu.cn (Q.-c. Zhang), jinzhao@mail.xjtu.edu.cn (F. Jin).

http://dx.doi.org/10.1016/j.compstruct.2017.03.045
0263-8223/

For large-scale sandwich structures with hybrid cores, it would be important to predict their natural frequencies. In recent years, homogenization equivalent methods have been widely used to obtain the equivalent model of some cellular structures [22–27]. Compared with tedious analytical methods and three dimensional detailed finite element methods (3D model) [22,23], the equivalent method can be used to improve the computational efficiency and further reduce the computational expense. Xia et al. [27] proposed such three equivalent methods as the honeycomb-plate theory, the sandwich theory and the equivalent-plate theory. It was shown that three equivalent methods were reliable and practical, and they can be used for predicting the natural frequencies of honeycomb-sandwich plates. Liu et al. [28,29] derived the effective stiffness matrix of corrugated and lattice truss cores. The equivalent models were used successfully for finite element analysis of characteristic modes. In comparison with the results obtained by three detailed finite element models, the equivalent approach can give acceptable predictions on dynamic behavior of sandwich panels. Yet until recently, Han et al. [15] studied the existing foam-filled corrugated hybrid cores, and obtained their equivalent elastic constants, and studied the vibration characteristics under thermal loading. However, newly honeycomb-corrugation hybrid cores for sandwich structures have rarely been investigated based upon the equivalent model. In this paper, based upon a micromechanics-based model, the effective elastic constants of honeycomb-corrugation hybrid core are derived by the homogenization method. The hybrid core is equivalent to a homogeneous medium used to constitute the equivalent model (2D model). In order to verify its accuracy, the three-dimensional finite element model (3D model) and experimental tests were carried out respectively to predict the vibration characteristics of sandwich structures with hybrid core under clamped-free boundary conditions. The influence of key geometrical parameters on their vibration performance is also explored.

2. Formulation of honeycomb-corrugation hybrid core homogenization

2.1. Homogenization

Based upon the micro-mechanical models with small elastic deformation, the honeycomb-corrugation hybrid cores are treated as homogeneous orthotropic materials as shown in Fig. 1. Geometric parameters of honeycomb-corrugation hybrid cores are: honeycomb cell length l_H, single wall thickness t_H, corrugated member length l_c, corrugation angle θ, the width of corrugation platform d, core height h_c, corrugated member thickness t_c, the sheet thickness t_f. ρ_s represents the density of the corrugated member and honeycomb material. Let E and v denote the Young's modulus and Poisson ratio.

The relative density $\bar{\rho}$ of the honeycomb-corrugation hybrid core is:

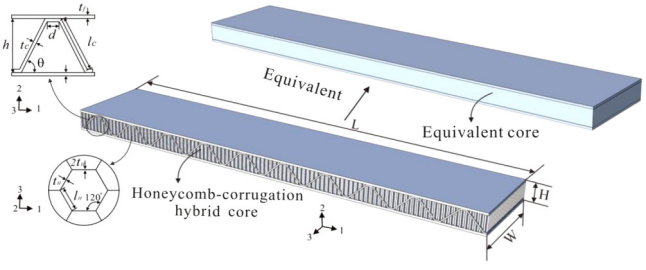

Fig. 1. Schematic diagram of sandwich beam with honeycomb-corrugation hybrid core transformed to equivalent one by homogenization method.

$$\bar{\rho} = \bar{\rho}_C + \bar{\rho}_H(1 - \bar{\rho}_C) \tag{1}$$

where $\bar{\rho}_H$ and $\bar{\rho}_C$ denote the relative density of the honeycomb and empty corrugation core, respectively, and λ is the volume fraction of hybrid core occupied by corrugation member, given by:

$$\bar{\rho}_H = \frac{8t_H}{3(\sqrt{3}l_H + 2t_H)} \cong \frac{8}{3\sqrt{3}}\frac{t_H}{l_H} \tag{2}$$

$$\bar{\rho}_C = \frac{t_c(d + l_c)}{(d + l_c\cos\alpha)(t_c + l_c\sin\theta)} \tag{3}$$

$$\lambda = \bar{\rho}_C \tag{4}$$

It is assumed that the corrugated members and the face sheets are welded together and no slip occurs when subjected to loading. Hence, the corrugated members are treated as Euler-Bernoulli beams with clamped support at both ends. It is further assumed that filling honeycomb and corrugated members keep close contact with each other during deformation. For small strain deformations, the deformation of the face sheets has negligible influence on the geometry of the unit cell.

The honeycomb-corrugation hybrid core may be analyzed at two different scales: (a) at the macro scale, the hybrid core is considered as a homogeneous continuum solid; (b) at the micro-scale, the corrugated members and filling honeycomb are separately considered. The derivation of micro-dium relies on the analysis of its representative volume element (RVE, or unit cell). The analysis parallels that of pin-reinforced foam cores [7] and foam-reinforced corrugated cores [15]. The macroscopic strain energy density of honeycomb-corrugation hybrid core may be written as:

$$U^* = U^C + U^H \tag{5}$$

$$U^C = \frac{1}{\Omega}\sum_{i=1}^{2}\left[\frac{1}{2}(\tilde{\mathrm{u}}^{(i)} + 2\tilde{\mathrm{u}}_{\mathrm{p}}^{(i)})^T\tilde{\mathrm{K}}^{(i)}\tilde{\mathrm{u}}^{(i)} - \tilde{g}_p^{(i)}\right] \tag{6}$$

$$U^H = (1-\lambda)\left(\frac{1}{2}C^H_{hjkl}E_{hj}E_{kl}\right) + \frac{1}{\Omega}\sum_{i=1}^{2}\tilde{g}_p^{(i)} \tag{7}$$

where U^C and U^H are the strain energy of the corrugated members and filling honeycomb, respectively. Ω denotes the volume of the unit cell. Superscript C and H represent the corrugation and the honeycomb, respectively.

2.2. Small strain kinematics

Consider the deformation of a unit cell comprising of a corrugated member surrounded by filling honeycomb and subjected to a $\bar{x}-\bar{z}$ plane macroscopic strain E as schematically shown in Fig. 2(a). The corrugated member in the $\bar{x}-\bar{z}$ plane can be treated as an Euler-Bernoulli beam of unit width, clamped at both ends. $\tilde{\mathrm{u}}^{(i)}$ is the global nodal displacement vector for the ith inclined beam characterized by end nodes ζ and τ (Fig. 2(b)):

$$\tilde{\mathbf{u}}^{(i)} = \mathbf{T}^{\mathrm{T}}\tilde{\mathbf{u}}^{(i)e} \tag{8}$$

$$\tilde{\mathbf{u}}^{(i)e} = [w_\zeta,\ v_\zeta, \theta_\zeta, w_\tau,\ v_\tau, \theta_\tau]^{(i)\mathrm{T}} \tag{9}$$

where $\tilde{\mathbf{u}}^{(i)e}$ denotes the nodal displacement vector under local coordinates (x,z), $\mathbf{T}$ is the transformation matrix between local and global coordinates (see Appendix A), and e represents values in local coordinates. The global nodal displacement vector for the ith beam can be written as:

$$\bar{u}^{(i)} = [\Delta_1, \Delta_2, 0, 0, 0, 0]^{(i)\mathrm{T}} \tag{10}$$

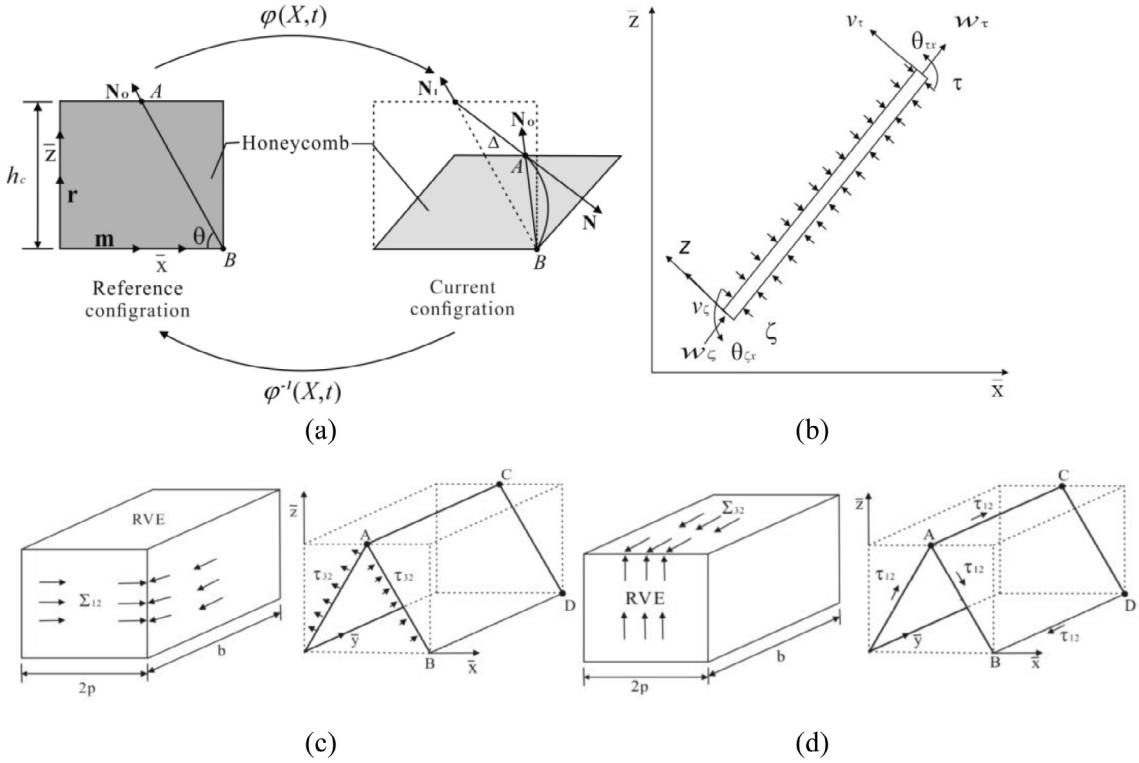

Fig. 2. Homogenization of honeycomb-corrugation hybrid core: (a) the kinematics of a inclined corrugated member; (b) an inclined corrugated member subjected to nodal forces/moments and lateral pressure; (c) shear flow in a typical cell and its representative volume element when: (c) macroscopic shear stress τ_{32} or (d) macroscopic shear stress τ_{12} is imposed.

Here, Δ_1 and Δ_2 denote the projections of the end node displacement Δ, given by

$$\Delta = \frac{h_c}{\sin\theta}\mathbf{E}\mathbf{N}_0 \tag{11}$$

where

$$\mathbf{E} = \begin{bmatrix} E_{22} & E_{23} \\ sym & E_{33} \end{bmatrix}, \quad \mathbf{\Delta} = (\Delta_1\mathbf{m}, \Delta_2\mathbf{r})^{\mathrm{T}} \tag{12}$$

Here, $\mathbf{N}_0$ denotes the unit vector along with which the inclined beam is initially aligned.

In Eq. (6), $\bar{\mathbf{u}}_p^{(i)}$ is the nodal displacement vector of the ith inclined beam contributed by lateral normal stress $p^{(i)}$ in Fig. 2(b):

$$\bar{\mathbf{u}}_p^{(i)} = \mathbf{T}^{\mathbf{T}}\bar{\mathbf{u}}_p^{(i)e} \tag{13}$$

$$\bar{\mathbf{u}}_p^{(i)e} = \left[\frac{yp^{(i)}}{E}l \quad 0 \quad 0 \quad 0 \quad 0 \quad 0\right]^{\mathrm{T}} \tag{14}$$

The effect of shear stress on the lateral surface of the inclined beam is ignored. The contribution of lateral normal stress $p^{(i)}$ to the strain energy just considers the elongation related to the inclined beam and the compression related to beam lateral surface.

The macroscopic deformation of filling honeycomb in a unit cell is approximately equal to that of the unit cell. Therefore, with close contact assumed between corrugated members and filling honeycomb, $p^{(i)}$ is assumed to be approximately uniformly distributed on the lateral surface of inclined beam, and can be obtained as:

$$p^{(i)} = \mathbf{n}_2^{\mathrm{T}}\begin{bmatrix} \sigma_{11} & \sigma_{12} & \sigma_{13} \\ \sigma_{21} & \sigma_{22} & \sigma_{23} \\ \sigma_{31} & \sigma_{32} & \sigma_{33} \end{bmatrix}^H \mathbf{n}_2 \tag{15}$$

$$\sigma^H = C^H E \tag{16}$$

where $\mathbf{n}_2$ is the unit vector normal to the lateral surface of the inclined beam. The stiffness matrix C^H of the honeycomb is given in Appendix B [26].

In Eq. (6), $\bar{\mathbf{K}}^{(i)}$ is the global stiffness matrix that satisfies the transformation between local and global coordinates:

$$\bar{\mathbf{K}}^{(i)} = \mathbf{T}^{\mathrm{T}}\bar{\mathbf{K}}^{e(i)}\mathbf{T} \tag{17}$$

where $\bar{\mathbf{K}}^{e(i)}$ is the elementary stiffness matrix of the ith beam, as given in Appendix A. The macroscopic strain vector of the unit cell may be defined as:

$$\begin{aligned}\mathbf{\Xi} &= [\,\Xi_1 \quad \Xi_2 \quad \Xi_3 \quad \Xi_4 \quad \Xi_5 \quad \Xi_6\,]^{\mathrm{T}} \\ &= [\,E_{11} \quad E_{22} \quad E_{33} \quad 2E_{23} \quad 2E_{13} \quad 2E_{12}\,]^{\mathrm{T}}\end{aligned} \tag{18}$$

The effective stiffness of the unit cell may be obtained by:

$$C_{ij}^* = \frac{\partial^2 U^*}{\partial\Xi_i\partial\Xi_j} \tag{19}$$

2.3. Macroscopic equivalent properties of honeycomb-corrugation hybrid core

Using Eqs. (18) and (19), the $\bar{x}-\bar{z}$ plane macroscopic effective stiffness C_{ij}^* of a honeycomb-corrugation hybrid core may be written as:

$$C_{11}^* = \frac{\lambda E}{(1-\nu^2)} + (1-\lambda)C_{11}^H \tag{20}$$

$$C_{33}^* = \frac{E}{(1-\nu^2)}\left(\frac{t}{l}\right)\frac{\sin^3\theta}{\cos\theta} + \frac{E}{(1-\nu^2)}\left(\frac{t}{l}\right)^3\sin\theta\cos\theta + (1-\lambda)C_{33}^H \tag{21}$$

$$C_{13}^{*}=\frac{E}{(1-\nu^2)}\left(\frac{t}{l}\right)\sin\theta\cos\theta-\frac{E}{(1-\nu^2)}\left(\frac{t}{l}\right)^3\sin\theta\cos\theta+(1-\lambda)C_{13}^{H} \tag{22}$$

$$C_{55}^{*}=\frac{E}{(1-\nu^2)}\left(\frac{t}{l}\right)\sin\theta\cos\theta+\frac{1}{4}\frac{E}{(1-\nu^2)}\left(\frac{t}{l}\right)^3\times\left(\frac{\sin^3\theta}{\cos\theta}+\frac{\cos^3\theta}{\sin\theta}-2\sin\theta\cos\theta\right)+(1-\lambda)C_{55}^{H} \tag{23}$$

The contribution of coupling effect derived from filling honeycomb and corrugated members is little and so has been neglected. The elastic stiffness just considers the contribution of stretching and bending deformation for the corrugated members and filling honeycomb.

If a macroscopic strain E_{22} is imposed on the unit cell, the local normal stress σ_y^c of a corrugated member and σ_y^H of filling honeycomb in the $\bar{y}$-direction are given by:

$$\sigma_y^c=\frac{E}{(1-\nu^2)}E_{22} \tag{24}$$

$$\sigma_y^H=C_{22}^{H}E_{22} \tag{25}$$

The macroscopic stress σ_y in the $\bar{y}$-direction is obtained:

$$\sigma_y=\lambda\sigma_y^c+(1-\lambda)\sigma_y^H \tag{26}$$

$$C_{22}^{*}=\lambda\frac{E}{(1-\nu^2)}+(1-\lambda)C_{22}^{H} \tag{27}$$

If E_{11} or E_{33} is solely imposed on the unit cell, the macroscopic stress σ_y can be obtained by using nodal displacements and the corresponding equilibrium equations. Consequently, C_{12}^{*} and C_{23}^{*} can be written as:

$$C_{12}^{*}=\frac{\lambda\nu E}{(1-\nu^2)}\frac{\cos\theta}{\sin\theta}+(1-\lambda)C_{12}^{H} \tag{28}$$

$$C_{23}^{*}=\frac{\lambda\nu E}{(1-\nu^2)}\frac{\sin\theta}{\cos\theta}+(1-\lambda)C_{23}^{H} \tag{29}$$

When subjected to a macroscopic shear strain E_{11} or E_{33} the resulting distributed shear flow in a unit cell is shown in Fig. 2 (c) or (d). The macroscopic shear stress Σ_{2i} can be written as:

$$\Sigma_{2i}=\Sigma_{2i}^{C}+\Sigma_{2i}^{H} \tag{30}$$

where Σ_{2i}^{C} and Σ_{2i}^{H} are macroscopic shear stress of corrugated member and filling honeycomb, respectively. In both cases, due to the symmetric layout of the unit cell, the local shear strains can be obtained as:

$$\varepsilon_{12}=\frac{\tau_{23}^{C}}{2G},\quad \varepsilon_{23}=\frac{\tau_{12}^{C}}{2G} \tag{31}$$

where G is shear modulus of the base material. Using micro-macro relations of energy equivalence, we have:

$$\frac{1}{2}C_{44}^{CH}(2E_{12})^2\Omega=\frac{1}{2}G\left(\frac{\tau_{23}^{C}}{G}\right)^2 tl \tag{32}$$

$$\frac{1}{2}C_{66}^{CH}(2E_{23})^2\Omega=\frac{1}{2}G\left(\frac{\tau_{12}^{C}}{G}\right)^2 tl \tag{33}$$

$$C_{ii}^{*}=C_{ii}^{CH}+(1-\lambda)C_{ii}^{H}(i=4,6) \tag{34}$$

Consequently, C_{44}^{*} and C_{66}^{*} can be written as:

$$C_{44}^{*}=G\left(\frac{t}{l}\right)\frac{\sin\theta}{\cos\theta}+(1-\lambda)C_{44}^{H} \tag{35}$$

$$C_{66}^{*}=G\frac{\sin\theta}{\cos\theta}+(1-\lambda)C_{66}^{H} \tag{36}$$

3. Experimental

3.1. Materials and fabrication

Considering a honeycomb-corrugation hybrid core sandwich structure in Fig. 3(a), the hybrid core is composed of aluminum corrugated member and trapezoidal A1 honeycomb blocks. The honeycomb blocks are made of A1-3003-H18, while the corrugated member and the face sheets are made of A1-3003-H24, their corresponding material properties are $E=70$ GPa, $\nu=0.3$ and $\rho=2700$ kg/m^3. The corrugated member was treated by the folding method. Trapezoidal honeycomb blocks precisely cut from a commercial honeycomb panel by electro-discharge machining was just right inserted into the interstices of the corrugated core. Finally, the sandwich beam was fabricated by inserting the honeycomb blocks into the corrugated core, fixed by epoxy glue, then adhesively bonded to the Al face sheets. The literature [21] describes detailedly the manufacturing process of sandwich beam. Geometrical dimensions of these beams used in test are illustrated in Table 1. The cells of corrugated core have been arranged in transverse and longitudinal directions. Two different kinds of specimens, *i.e.* beam I and beam II, were prepared and tested in this experiment as shown in Fig. 3(b), wherein beam I contains two hybrid cells in the width direction, and beam II contains ten hybrid cells in the length direction.

3.2. Experimental process

Modal testing was performed on sandwich beam under clamed-free boundary condition. The first three natural frequencies and the corresponding mode shapes of sandwich beam were reported. Experimental equipment consisted of an impact hammer, a B&K type accelerometer, a charge amplifier, a clamping system and a LMS-Test-Lab modal analysis system as shown in Fig. 4. The experiment was carried out by multi-point excitation and single point measurement. First, the specimen was fixed at one end by means of the clamping system. Then twenty excitation points were evenly arranged on the specimens as shown in Fig. 3(b). The point-by-point excitation method was used by the impact hammer. The impact force-time history from the hammer was recorded by the force transducer connected with the impact hammer. The vibration response of specimen was detected using acceleration transducer. The signals gotten from force transducer and acceleration transducer were processed by LMS-Test-Lab modal analysis system. Frequency response analysis was carried out to obtain the natural frequencies and mode shapes. The average values of three tests were reported in the present study.

4. Finite element modeling

Vibration characteristics of sandwich beam having honeycomb-corrugation hybrid core are analyzed by using such finite element methods as the equivalent model (2D model) and the three-dimensional finite element model (3D model). The commercial finite element code ABAQUS/Standard is employed to obtain the natural frequencies and the mode shapes of sandwich beams. Eight-node linear brick elements with reduced integration (C3D8R) are used for both the face sheets and the corrugated members in 3D or 2D models. Linear quadrilateral shell elements with

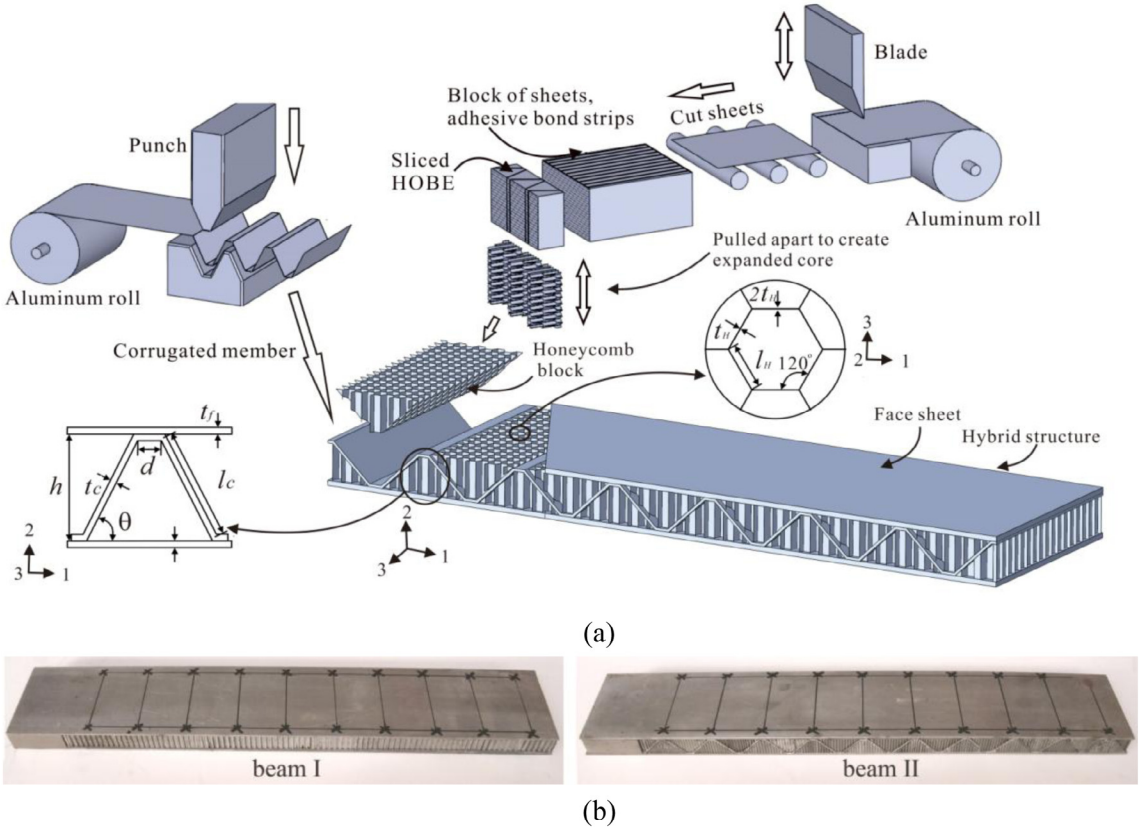

Fig. 3. (a) Schematic of the fabrication process of sandwich beam with honeycomb-corrugation hybrid core, (b) specimens of beam I and beam II denote longitudinally and transversely corrugated core sandwich beams with honeycomb insertion, respectively.

Table 1
Geometrical dimensions of sandwich beam (mm).

L	H	W	l_H	t_H	l_c	h_c	t_c	θ	d	t_f
300	14.2	60	1	0.06	15.4	11.4	0.6	45°	3.6	1.4

induced integration (S4R) are just used for filling honeycomb in 3D models. A mesh convergence study was carried out to make the mesh refinement fine enough on the numerical result even though further refining of the mesh. The mesh grid is one over ten of the height of sandwich beam. A linear perturbation analysis step is created, and frequency extraction procedure is carried out with the lanczos solver. All parts are considered to be perfectly bonded together.

5. Results and discussions

5.1. Validate and analysis

The first three natural frequencies of two different sandwich beams have been obtained by 2D numerical model, 3D numerical model and experimental tests in Table 2. The results obtained from the analysis of 2D numerical model meet good agreement with ones from 3Dnumericalmodel and experimental tests. The first three mode shapes of 2D numerical model are consistent with

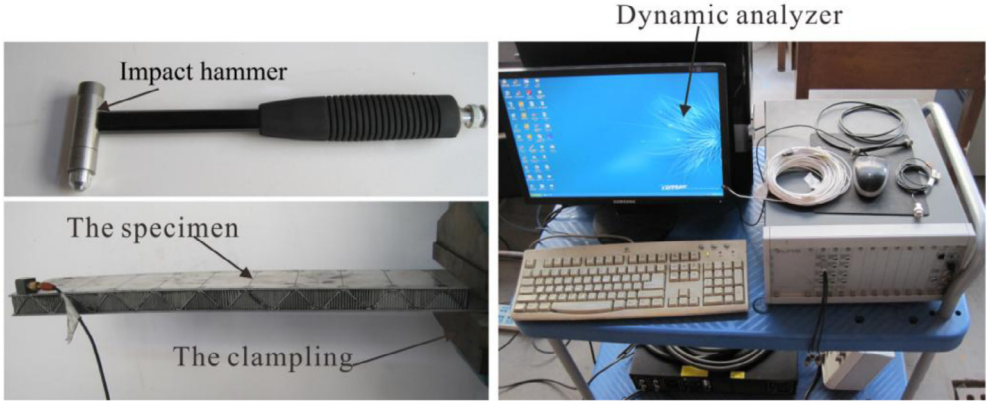

Fig. 4. Test setup of modal testing.

Table 2
The first three natural frequencies of sandwich beams obtained by three different methods (Hz).

Order	Beam I			Beam II		
	Experimental value	3D model value	2D model value	Experimental value	3D model value	2D model value
f_1	153	162	158	150	156	154
f_2	454	482	463	435	453	441
f_3	874	952	945	864	939	879

those of 3D numerical model and experimental tests as shown in Fig. 5, wherein the first and third mode shapes are the bending mode, and the second mode shape is a lateral mode (the first three modal shapes of beam II are similar, so here is not given). For 2D model, its first two natural frequencies for both sandwich beams is less 5% than those of two other models, and its third natural frequency shows a significant difference at less 10% error than those of two other models. The experimental result is lower than that of the 2D model, due to the effect of adhesive mass. The 3D model result is higher than the 2D model one, mainly because of the ignored coupling effect of hybrid core in the 2D model. In addition, the first three natural frequencies of beam I derived from three methods are a little higher than those of beam II, despite the same weight. This is mainly because the stiffness of longitudinally corrugated core sandwich beam is higher than that of transversely corrugated core sandwich beam.

5.2. Effect of honeycomb insertion on the vibration characteristics of sandwich beams

In this section, the vibration characteristics of sandwich beams with corrugated core, honeycomb core and hybrid core are discussed. The first four natural frequencies and corresponding mode shapes of vibrations of the sandwich beams are presented in Fig. 6. In the corresponding order, it is noted that the frequency of hybrid core sandwich beam is the maximum, the frequency of corrugated core sandwich beam is minimal, which means the bending stiffness of sandwich beam with hybrid core is the maximum at nominally the same mass. Moreover, the localized vibration mode shapes appear the between second and fourth mode for longitudinally corrugated core sandwich beam, and the third and the fourth mode for transversely corrugated core sandwich beam II. Nevertheless, the localized vibration modes do not appear for honeycomb core sandwich beam and hybrid core sandwich beam. It is due to the fact that the corrugated members in the honeycomb-corrugation hybrid core sandwich beam are considerably stabilized by the filling honeycomb against lateral deflection. The mutual constraint between corrugated member and honeycomb cell walls results in improving the stiffness and inhibiting the local vibration mode of sandwich beam.

Due to serious anisotropy of mechanical properties of corrugated core sandwich structure, it is easily found that the first natural frequency of longitudinally corrugated core sandwich beam is 27.2% higher than that of transversely corrugated core sandwich beam. However, the first natural frequency of sandwich beam I is just 3% higher than that of sandwich beam II as shown in Fig. 7. Filling honeycomb weakens the directivity of the stiffness of corrugated core sandwich beam.

5.3. Effects of geometric parameters on the vibration characteristics of sandwich beam with honeycomb-corrugation hybrid core

Effects of such geometry parameters as the face sheet thickness ratio t_f/h_c, the relative density of filling honeycomb $\bar{\rho}$, the slenderness ratio of corrugated member t_c/l_c, and the inclination angle θ on the first natural frequency of sandwich beam are discussed further using FEM with ABAQUS/Standard. With material parameters fixed, the geometric parameters of the sandwich are varied. To

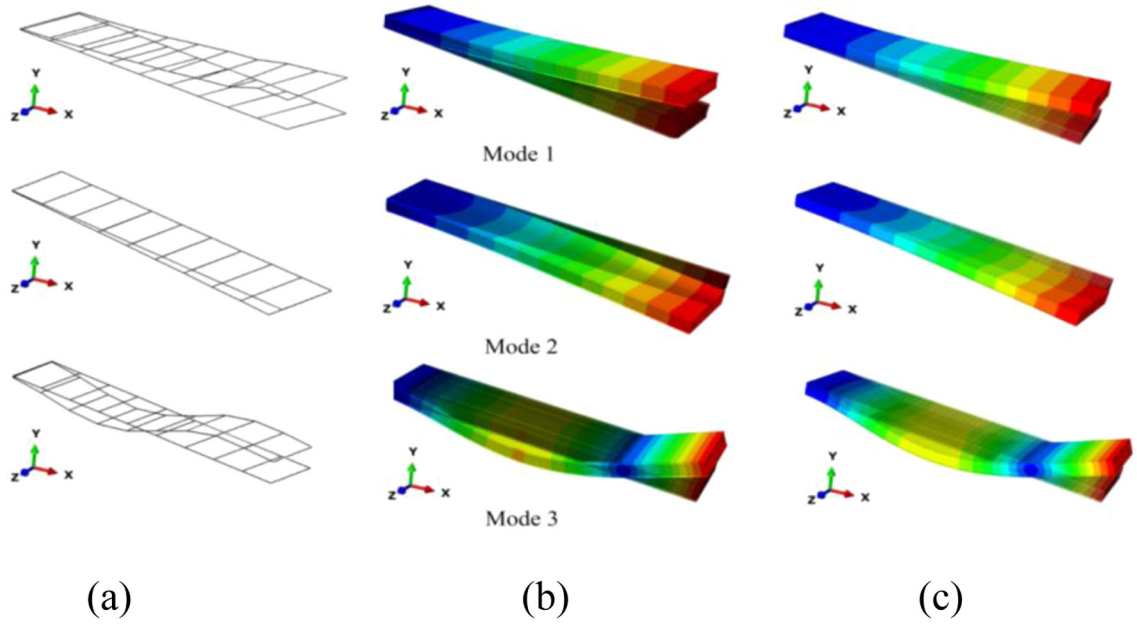

Fig. 5. The first three modal shapes deduced from (a) experimental test; (b) 3D model for longitudinal corrugation core sandwich beam with honeycomb insertion; (c) 2D model for sandwich beam with equivalent core.

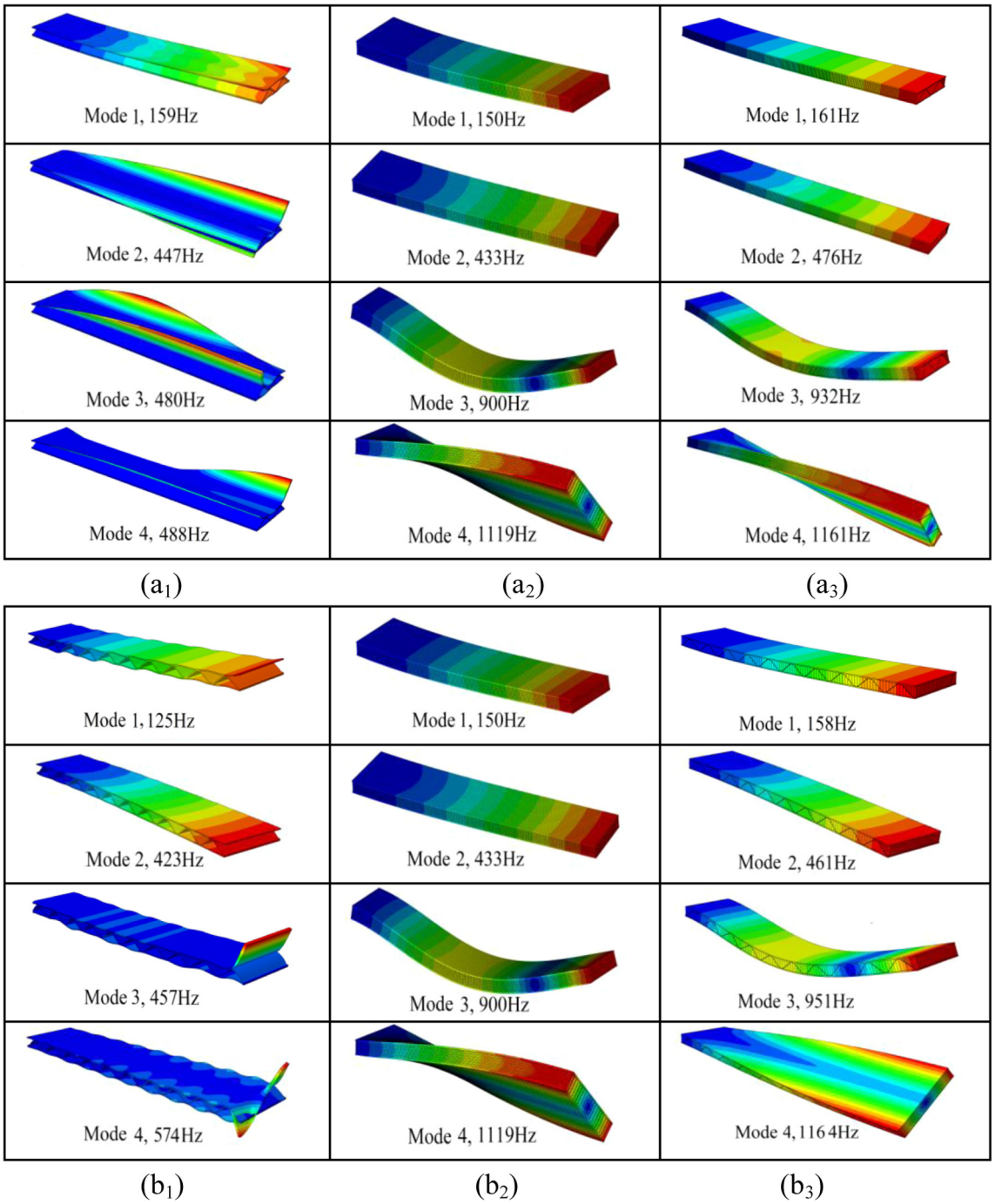

Fig. 6. Comparison of first four mode shapes of sandwich beam with (a_1) empty longitudinally corrugated core, (a_2) honeycomb core, (a_3) hybrid core I; sandwich beam with (b_1) transversely empty corrugated core, (b_2) honeycomb core, (b_3) hybrid core II.

reveal the superiority of hybrid sandwich beams over the solid beams, a dimensionless parameter is proposed as ω/ϖ, where ω and ϖ are the first natural frequency of the sandwich beam and the corresponding solid beam with the same length, width, weight and boundary condition, respectively. The height of solid beam can be obtained:

$$h = \bar{\rho} h_c + 2t_f \tag{37}$$

The first natural frequency of a solid beam is given [24]:

$$\varpi = \frac{1.01}{2\pi}\sqrt{\frac{Eh^2}{\rho L^4}} \tag{38}$$

Fig. 8 illustrates the effects of geometric parameters on ω/ϖ of both the sandwich beam I and beam II. In Fig. 8(a), it is showed that ω/ϖ decreases with the increase of face sheet thickness ratio t_f/h_c. It is the well-known that face sheets play an important role in promoting the bending stiffness of sandwich beam [22]. The mass of sandwich beam increases with the increase of t_f/h_c, which leads to an increase in the natural frequency. At the same time, the natural frequencies of the corresponding solid beams also increase with t_f/h_c as shown in Table 3,which leads to a decreased ω/ϖ. As for the relative density of filling honeycomb, the slenderness ratio of corrugated member and the inclination angle of corrugated member, they all have the similar influence on nature frequency, as

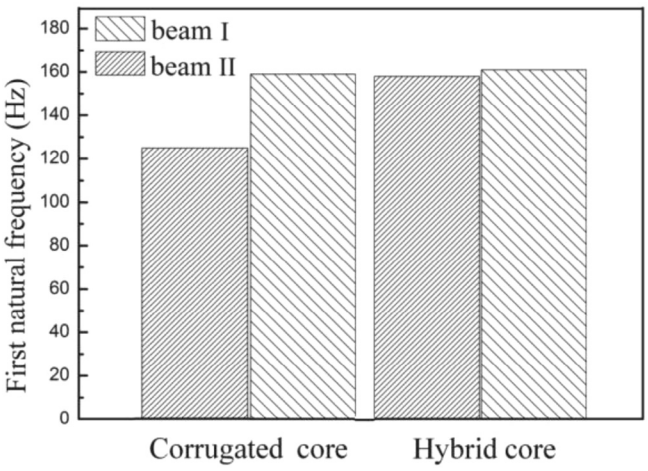

Fig. 7. Comparison of first natural frequency of sandwich beams with hybrid cores and empty corrugated cores.

illustrated in Fig. 8(b)–(d). As the relative density of filling honeycomb, the slenderness ratio of corrugated member and the inclination angle of corrugated member increase, both the mass and structural stiffness of sandwich beam increase. Compared with the structural stiffness, the mass plays a dominant role on the

Table 3
The effects of geometric parameters on the natural frequency of sandwich beams and the corresponding solid beams (HZ).

Varied geometrical parameter	Beam I		Beam II		Solid beam
	FEM	Equivalent	FEM	Equivalent	
Effect of face sheet thickness t_f/h_c					
0.04	142	136	135	135	22
0.08	163	158	158	157	31
0.12	177	172	175	174	40
0.15	188	184	187	186	49
0.18	199	197	198	194	58
Effect of the relative density of honeycomb $\bar{\rho}$					
0.03	183	182	180	178	36
0.06	177	176	175	172	38
0.09	171	169	170	168	42
0.12	167	165	165	163	45
0.15	162	160	160	155	48
Effect of the slenderness ratio t_c/l_c					
0.01	167	166	166	165	27
0.021	163	162	161	160	28
0.033	160	159	157	155	30
0.047	158	157	153	151	33
0.06	155	155	148	147	36
Effect of the angle of corrugated member θ					
40	157	153	150	147	34
45	156	150	149	146	34
50	155	148	148	146	35
55	154	147	146	145	35
60	152	146	145	144	35

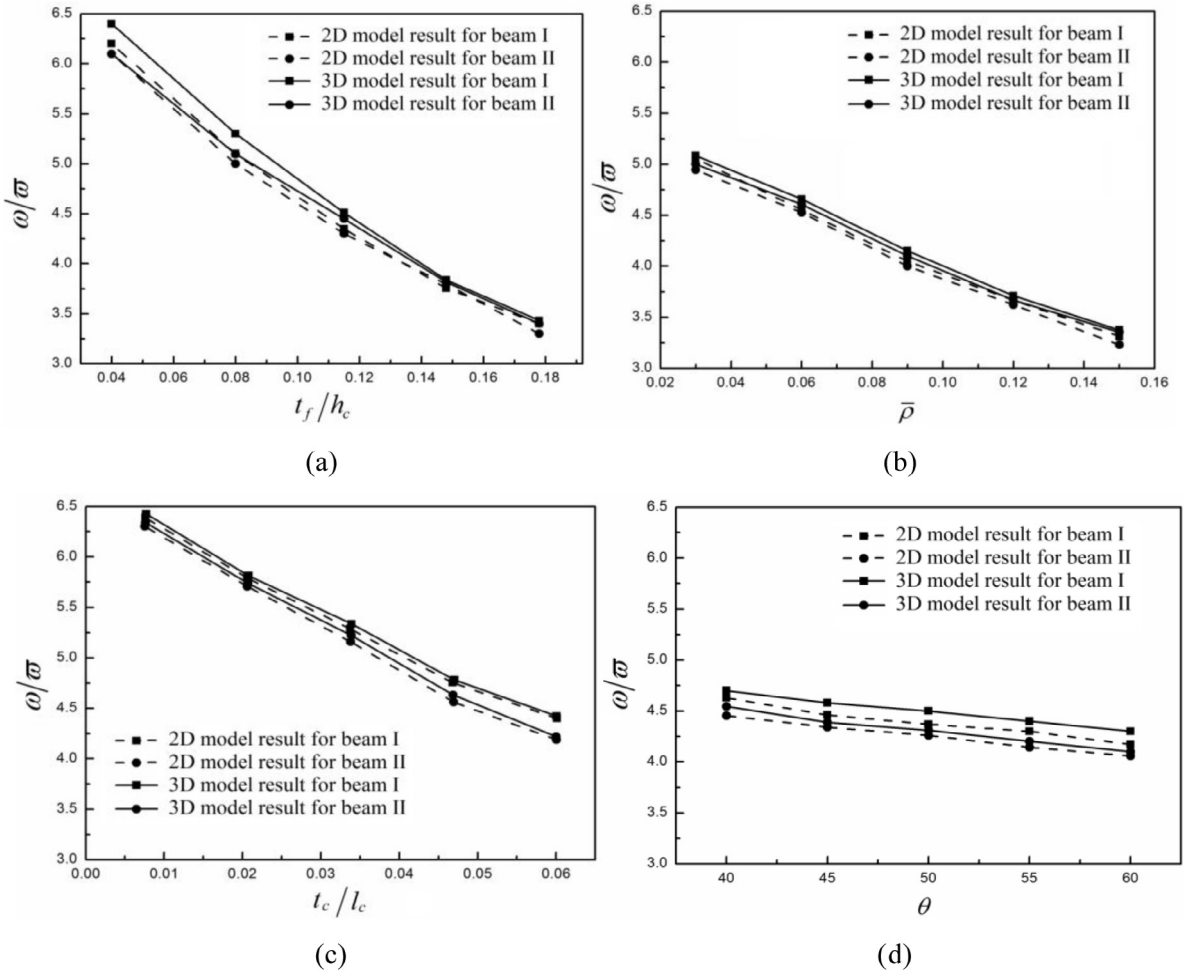

Fig. 8. Effects of geometric parameters on the dimensionless frequency parameter $\bar{\rho}$ of sandwich beam I and beam II: (a) the face sheet thickness ratio t_f/h_c; (b) the relative density of filling honeycomb $\bar{\rho}$; (c) the slenderness ratio of corrugated member t_c/l_c; (d) the inclination angle of corrugated member θ.

frequency parameters of sandwich beam. The natural frequency of sandwich beams decrease as shown in Table 3, resulting in the descending of ω/ϖ. In addition, compared with the face sheet thickness ratio, the effects of the relative density of filling honeycomb and the slenderness ratio of corrugated member on the frequency parameter slightly decease. However, the frequency parameter is insensitive to the inclination angle of corrugated member as shown in Fig. 8(d).

6. Conclusion

The equivalent elastic constants of equivalent model of honeycomb-corrugation hybrid core have been derived employing the homogenization method. The equivalent model (2D numerical model) has been used to predict the vibration characteristic of sandwich beams. In comparison with results obtained by using 3D numerical model and experimental tests, the equivalent model can give acceptable predictions for mode analysis of sandwich beam with honeycomb-corrugation hybrid cores. Moreover, it was found the filling honeycomb had an effect on weakening the anisotropy of the stiffness and suppressing the local mode shape for sandwich beam. The geometry parameters have an effect on the vibration characteristics of sandwich beam with hybrid core. The effect of face sheet thickness on the frequency parameter is the greatest, and the frequency parameter is not sensitive to the inclination angle of corrugated member. This work is helpful for researchers in design for the practical application of the honeycomb-corrugation hybrid-cored sandwich structures.

Acknowledgements

This work was supported by the National Natural Science Foundation of China (11472209), the Fundamental Research Funds for Xi'an Jiaotong University (xjj2015102), China Postdoctoral Science Foundation (2016M600782), and Postdoctoral Scientific Research Project of Shaanxi Province (2016BSHYDZZ18).

Appendix A

For Euler-Bernoulli beams, the elementary stiffness matrix is:

$$\mathbf{K}^{e(i)} = \begin{bmatrix} \frac{EA}{l} & 0 & 0 & -\frac{EA}{l} & 0 & 0 \\ 0 & \frac{12EI}{l^3} & \frac{6EI}{l^2} & 0 & -\frac{12EI}{l^3} & \frac{6EI}{l^2} \\ 0 & \frac{6EI}{l^2} & \frac{4EI}{l} & 0 & -\frac{6EI}{l^2} & \frac{2E_sI}{l} \\ -\frac{EA}{l} & 0 & 0 & \frac{EA}{l} & 0 & 0 \\ 0 & -\frac{12EI}{l^3} & -\frac{6EI}{l^2} & 0 & \frac{12EI}{l^3} & -\frac{6EI}{l^2} \\ 0 & \frac{6EI}{l^2} & \frac{2EI}{l} & 0 & -\frac{6EI}{l^2} & \frac{4EI}{l} \end{bmatrix} \tag{A1}$$

where A and I are the cross-sectional area and moment of inertia of the beam, respectively.

The transformation matrix between local and global coordinates for one corrugated member as shown in Fig. 2(a) is given by:

$$\begin{bmatrix} \cos\theta & \sin\theta & 0 & 0 & 0 & 0 \\ -\sin\theta & \cos\theta & 0 & 0 & 0 & 0 \\ 0 & 0 & 1 & 0 & 0 & 0 \\ 0 & 0 & 0 & \cos\theta & \sin\theta & 0 \\ 0 & 0 & 0 & -\sin\theta & \cos\theta & 0 \\ 0 & 0 & 0 & 0 & 0 & 1 \end{bmatrix} \tag{A2}$$

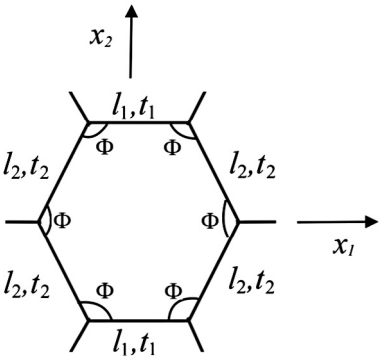

Fig. 1B. Hexagonal honeycomb core.

Appendix B

The geometry is described by the length l_1 and thickness t_1 of the cell wall, the length l_2 and thickness t_2 of the inclined cell walls and the cell angle ϕ (see Fig. 1B). Due to the manufacturing process, the thickness t_1 of horizontal cell wall is usually twice thickness t_2 of the inclined cell wall.

The elastic constants of filling honeycomb are [26]:

$$C_{11}^H = E\frac{t_1 l_1\left(1-\frac{\gamma_1}{\beta}\right)-2t_2 l_2\left(\frac{\gamma_1}{\beta}-\cos\Phi\right)\cos^3\Phi}{12 l_2(l_1-l_2\cos\Phi)\sin\Phi}$$

$$C_{12}^H = E\frac{-t_2\left(\frac{l_1\gamma_1}{l_2\beta}-\cos\Phi\right)\sin\Phi\cos\Phi}{l_1-l_2\cos\Phi}$$

$$C_{13}^H = 0$$

$$C_{22}^H = E\frac{t_2\left(\sin^2\Phi+\frac{l_1\gamma_1}{l_2\beta}\cos\Phi\right)\sin\Phi}{l_1-l_2\cos\Phi}$$

$$C_{23}^H = 0$$

$$C_{33}^H = E\frac{t_1 l_1+2t_2 l_2}{2l_2(l_1-l_2\cos\Phi)\sin\Phi}$$

$$C_{44}^H = G\frac{t_2\sin\Phi}{l_1-l_2\cos\Phi}$$

$$C_{55}^H = G\frac{t_1 l_1+2t_2 l_2\cos^2\Phi-\frac{t_1 l_1+2t_2 l_2\cos^2\Phi}{t_1 l_1+2t_2 l_2}(t_1 l_1+2t_2 l_2\cos^2\Phi)}{2l_2(l_1-l_2\cos\Phi)\sin\Phi}$$

$$C_{66}^H = E\frac{(l_1-l_2\cos\Phi+l_1\sin^2\Phi)\left(1-\frac{l_1}{l_2}\cos\Phi+\frac{l_1}{l_2}\frac{1}{\gamma_6}\cos\Phi-\frac{2}{\gamma_6}\cos^2\Phi\right)}{2l_2(l_1-l_2\cos\Phi)\sin\Phi}$$

$$\gamma = 1+\frac{2(1+\nu)t_2^2}{l_2^2}$$

$$\gamma_1 = 1+2\frac{t_2^2}{l_2^2}\cos^3\Phi+2\frac{t_2}{t_1}\frac{t_2^2}{l_1^2}\frac{1}{\gamma}\sin\Phi\cos\Phi$$

$$\gamma_2 = 2\frac{t_2}{t_1}\left(\sin\Phi-\frac{t_2^2}{l_2^2}\frac{1}{\gamma}\right)\sin\Phi\cos\Phi$$

$$\gamma_6 = 1-\frac{l_1}{l_2}\cos\Phi$$

$$\beta = 1+2\frac{l_2}{t_2}\frac{t_1}{l_1}\cos^2\Phi+\frac{l_2}{t_2}\frac{t_1}{l_1}\frac{2t_2^2}{(1-\nu^2)l_2^2\gamma}\sin^2\Phi$$

$$\beta_6 = \frac{l_1^2}{2t_1^3\gamma_6}\left(2+\frac{l_2}{t_2^3}\frac{t_1^3}{l_1}\right)+\frac{2(1-\nu)}{t_1\gamma_6}\left(\gamma_6+\frac{1}{2}\frac{l_1}{t_2}\frac{t_1}{l_2}+\cos^2\Phi\right)+2\frac{\gamma_6}{3(1-\nu^2)\sin^2\Phi}\frac{l_2}{t_2 l_1} \tag{A3}$$

References

[1] Zhang QC, Yang XH, Li P, Huang GY, Feng SS, Shen C, et al. Bioinspired engineering of honeycomb structure – using nature to inspire human innovation. Prog Mater Sci 2015;74:332–400.
[2] Dayyani I, Shaw AD, Flores EI, Friswell MI. The mechanics of composite corrugated structures: a review with applications in morphing aircraft. Compos Struct 2015;133:358–80.
[3] Côté F, Deshpande VS, Fleck NA, Evans AG. The compressive and shear responses of corrugated and diamond lattice materials. Int J Solids Struct 2006;43(20):6220–42.
[4] Zhang QC, Han YJ, Chen CQ, Lu TJ. Ultralight X-type lattice sandwich structure (I): concept, fabrication and experimental characterization. Sci China Ser E: Technol Sci 2009;52(8):2147–54.

[5] Zhang QC, Chen AP, Chen CQ, Lu TJ. Ultralight X-type lattice sandwich structure (II): micromechanics modeling and finite element analysis. Sci China Ser E: Technol Sci 2009;52(9):2670–80.
[6] Han B, Zhang ZJ, Zhang QC, Zhang Q, Lu TJ, Lu BH. Recent advances in hybrid lattice-cored sandwiches for enhanced multifunctional performance. Extreme Mech Lett; 2016.
[7] Cartié DD, Fleck NA. The effect of pin reinforcement upon the through-thickness compressive strength of foam-cored sandwich panels. Compos Sci Technol 2003;63(16):2401–9.
[8] Marasco AI, Cartié DDR, Partridge IK, Rezai A. Mechanical properties balance in novel Z-pinned sandwich panels: Out-of-plane properties. Compos A Appl Sci Manuf 2006;37(2):295–302.
[9] Rice MC, Fleischer CA, Zupan M. Study on the collapse of pin-reinforced foam sandwich panel cores. Exp Mech 2006;46(2):197–204.
[10] Hammetter CI, Zok FW. Compressive response of pyramidal lattices embedded in foams. J Appl Mech 2014;81(1):011006.
[11] Ostos JB, Rinaldi RG, m Hammetter C, Stucky GD, Zok FW, Jacobsen AJ. Deformation stabilization of lattice structures via foam addition. Acta Mater 2012;60(19):6476–85.
[12] Vaziri A, Xue Z, Hutchinson JW. Metal sandwich plates with polymer foam-filled cores. J Mech Mater Struct 2006;1(1):97–127.
[13] Han B, Yu B, Xu Y, Chen CQ, Zhang QC, Lu TJ. Foam filling radically enhances transverse shear response of corrugated sandwich plates. Mater Des 2015;77:132–41.
[14] Yazici M, Wright J, Bertin D, Shukla A. Experimental and numerical study of foam filled corrugated core steel sandwich structures subjected to blast loading. Compos Struct 2014;110:98–109.
[15] Han B, Qin KK, Yu B, Zhang CQ, Chen CQ, Lu TJ. Design optimization of foam-reinforced corrugated sandwich beams. Compos Struct 2015;130:51–62.
[16] Nia AA, Sadeghi MZ. The effects of foam filling on compressive response of hexagonal cell aluminum honeycombs under axial loading-experimental study. Mater Des 2010;31(3):1216–30.
[17] Ahmad Z, Thambiratnam DP. Crushing response of foam-filled conical tubes under quasi-static axial loading. Mater Des 2009;30(7):2393–403.
[18] Yan LL, Yu B, Han B, Chen CQ, Zhang QC, Lu TJ. Compressive strength and energy absorption of sandwich panels with aluminum foam-filled corrugated cores. Compos Sci Technol 2013;86:142–8.
[19] Yan LL, Han B, Yu B, Chen CQ, Zhang QC, Lu TJ. Three-point bending of sandwich beams with aluminum foam-filled corrugated cores. Mater Des 2014;60:510–9.
[20] Han B, Yan LL, Yu B, Zhang QC, Chen CQ, Lu TJ. Collapse mechanisms of metallic sandwich structures with aluminum foam-filled corrugated cores. J Mech Mater Struct 2014;9(4):397–425.
[21] Han B, Qin KK, Yu B, Wang WB, Zhang CQ, Lu TJ. Honeycomb-corrugation hybrid as a novel sandwich core for significantly enhanced compressive performance. Mater Des 2016;93:271–82.
[22] Xu M, Qiu Z. Free vibration analysis and optimization of composite lattice truss core sandwich beams with interval parameters. Compos Struct 2013;106:85–95.
[23] Yang JS, Xiong J, Ma L, Wang B, Zhang GQ, Wu LZ. Vibration and damping characteristics of hybrid carbon fiber composite pyramidal truss sandwich panels with viscoelastic layers. Compos Struct 2013;106:570–80.
[24] Boudjemai A, Amri R, Mankour A, Salem H, Bouanane MH, Boutchicha D. Modal analysis and testing of hexagonal honeycomb plates used for satellite structural design. Mater Des 2012;35:266–75.
[25] Buannic N, Cartraud P, Quesnel T. Homogenization of corrugated core sandwich panels. Compos Struct 2003;59(3):299–312.
[26] Hohe J, Becker W. Effective stress-strain relations for two-dimensional cellular sandwich cores: homogenization, material models, and properties. Appl Mech Rev 2002;55(1):61–87.
[27] Xia LJ, Jin X, Wang YB. Equivalent analysis of honeycomb sandwich plates for satellite structure. J-Shanghai Jiaottong Univ-Chin Ed 2003;37(7):0999–1001.
[28] Liu T, Deng ZC, Lu TJ. Minimum weights of pressurized hollow sandwich cylinders with ultralight cellular cores. Int J Solids Struct 2007;44(10):3231–66.
[29] Liu T, Deng ZC, Lu TJ. Structural modeling of sandwich structures with lightweight cellular cores. Acta Mech Sin 2007;23(5):545–59.